

Time-resolved grazing-incidence small-angle X-ray scattering studies of lipid multibilayers with the insertion of amyloid peptide during the swelling process

Jhih-Min Lin,^a Tsang-Lang Lin^{a*} and U-Ser Jeng^b

^aDepartment of Engineering and System Science, National Tsing Hua University, Hsinchu 300, Taiwan, and

^bNational Synchrotron Radiation Research Center, Hsinchu 300, Taiwan. Correspondence e-mail: tllin@mx.nthu.edu.tw

The β -amyloid peptide ($A\beta$) (1–40) is one of the major components that form Alzheimer's amyloid deposits. Studies of the membrane insertion of amyloid showed that amyloid is surface active and can insert into lipid monolayers [Ji *et al.* (2002). *Biochemistry (Moscow)*, **67**, 1283–1288; Ege & Lee (2004). *Biophys. J.* **87**, 1732–1740]. The interaction between the peptide and a lipid monolayer or bilayer is critical to the understanding of the formation of amyloid peptide deposits on the membrane. In this paper, we have studied the structural transition of 1,2-dipalmitoyl-sn-glycero-3-phosphocholine (DPPC) multibilayers with the insertion of amyloid peptide 1–40 by grazing-incidence small-angle X-ray scattering at different bilayer hydration levels (changing the relative humidity). We mixed the DPPC and amyloid peptide in an organic solvent at a 10 to 1 weight ratio, then cast it onto a silicon wafer to form the mixed lipid multibilayer film. In this study of the pure DPPC multibilayer film and the DPPC multibilayer film inserted with amyloid peptide, it was found that the hydration process was bimodal with a better-hydrated top layer and a less-hydrated bottom layer. The gel-to-ripple phase transition suffers a strong confinement effect due to the presence of the solid substrate. With the insertion of the amyloid peptide, the ripple phase of the membrane bilayers was suppressed at high humidity and the whole film can be swollen more uniformly at lower incubation time than the pure DPPC film supported on a silicon wafer. This means water vapor can penetrate more easily into the DPPC bilayers inserted with $A\beta$ than into the pure DPPC bilayers. Amyloid peptides were found to form clusters in the bilayer and possess in-plane correlation. From analyzing the diffuse scattering around the Bragg peak in the lateral direction, the amyloid peptides are found to form clusters in the bilayer with a radius of about 9 nm. It is also estimated that the number of $A\beta$ molecules in one cluster is about 12 and on average each $A\beta$ molecule occupies an interface area of about 22 nm². As the relative humidity exceeds about 94%, the $A\beta$ clusters seem to develop an ordered structure with a spacing of about 300 Å.

© 2007 International Union of Crystallography
Printed in Singapore – all rights reserved

1. Introduction

The β -amyloid peptides ($A\beta$ s) are fragments derived from proteolytic cleavage of the large amyloid precursor protein (APP). The results of X-ray diffraction and nuclear magnetic resonance studies showed fibril aggregates can be formed by stacking pleated β -sheets of $A\beta$ (Li *et al.*, 1999). There are many factors that can affect the growth of the β -amyloid peptide aggregates. The concentration of the β -amyloid peptide is one of the most important factors. In the study of Lomakin *et al.* (1996), it was found that there was a critical concentration for the growth of β -amyloid peptide fibrils. Below the critical concentration the growth is heterogeneous and at greater than the critical concentration the growth is homogeneous. pH values can also affect the fibril growth rate (Wood *et al.*, 1996; Huang *et al.*,

2000). The interaction of $A\beta$ with lipid membranes is one of the key factors for their neurotoxicity. The presence of charged lipid vesicles could induce the transition from α -helix to β -sheet and the formation of aggregates. The interaction between the peptide and lipid monolayers and bilayers is critical to the understanding of the formation of amyloid peptide deposits on the membrane. Studies of the membrane insertion of amyloid showed that amyloid is surface active and can insert into lipid monolayers (Ji *et al.*, 2002; Ege & Lee, 2004). The study by Ege & Lee (2004) showed that the presence of amyloid in the subphase could induce morphology changes of the lipid monolayer. The experimental results showed that $A\beta$ can significantly increase the surface pressure of the monolayer and indicate the strong surface activity of $A\beta$. Lin *et al.* (2001) used atomic force microscopy (AFM) to observe the conformation of $A\beta$ inserted in the

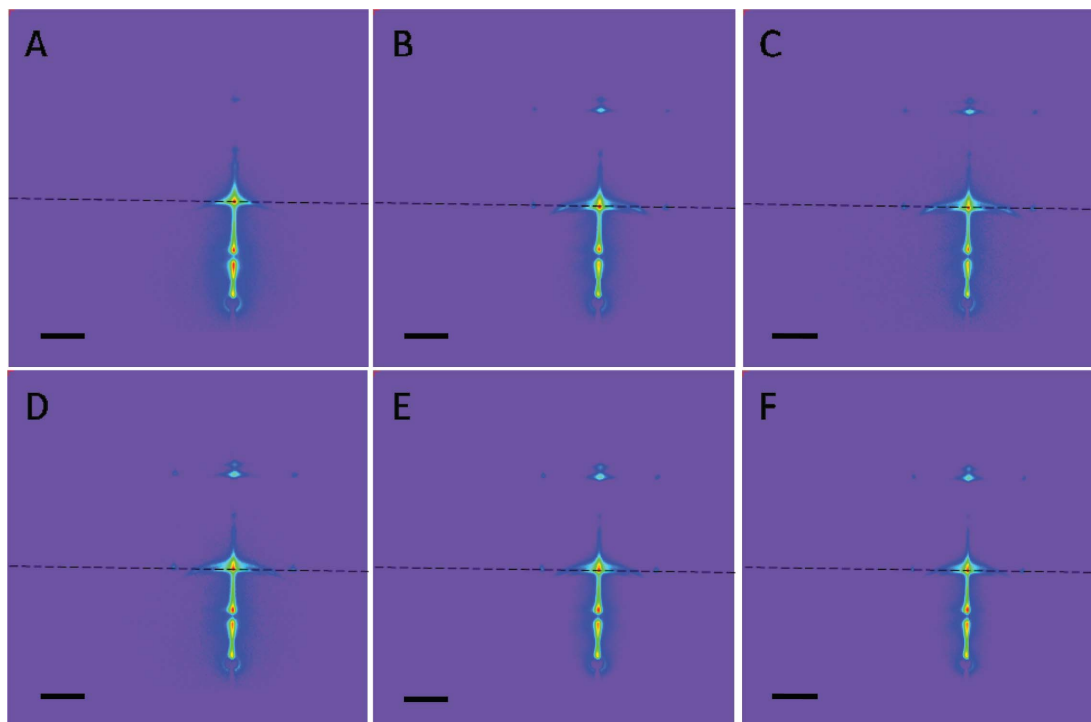


Figure 1
Grazing-incidence X-ray scattering patterns of DPPC multibilayers cast on a silicon wafer at about 306 K under different humidities: (A) RH = 36%, (B) RH = 81.38%, (C) RH = 85.58% (D) RH = 88.2% (E) RH = 90.2% and (F) RH = 93.88%. The dashed lines are the cuts for the intensity distribution profiles shown in Fig. 3(a). The length of the scale bar is 2.5 cm.

lipid bilayer. The AFM images of A β 1–42 reconstituted in a planar lipid bilayer reveals multimeric channel-like structures. Oligomeric A β has channel-like structures and donut-shaped structures with an outer diameter of 8–12 nm. There is a centralized pore-like depression and oligomeric walls protruding (~1 nm) above the embedding lipid bilayer surface. In the off-line zoomed images of the individual A β channel structures, two kinds of channels were observed. One is a rectangular structure with four apparent subunits and another is a hexagonal structure with six apparent subunits. According to these studies on the surface or the interface of a lipid monolayer or bilayer, it is certain that A β can be inserted into lipid bilayers. The insertion of the A β in the lipid bilayer would have significant effects on the physical and structural properties of the lipid bilayers. It is essential to understand how the membrane properties are affected by the presence of A β . Studies employing X-ray scattering, grazing-incidence small-angle X-ray scattering (GISAXS) and specular and diffusion diffraction to investigate the structures of oriented membranes and polymer thin films have been carried out (Salditt *et al.*, 1994; Koltover *et al.*, 1998; Vogel *et al.*, 2000; Salditt *et al.*, 2003; Spaar *et al.*, 2004; Lee *et al.*, 2005). Previously, we have successfully investigated the structural changes of lipid membranes due to the incorporation of fullerenes and fullerene derivatives by grazing-incidence X-ray scattering methods (Jeng *et al.*, 2005). Here, similar methods are used to investigate the structural transition of 1,2-dipalmitoyl-sn-glycero-3-phosphocholine (DPPC) multibilayer with the insertion of A β 1–40 by GISAXS at different bilayer hydration levels by changing the relative humidity.

2. Experimental

β -Amyloid peptide (A β) 1–40 with a molecular weight $M_w = 4329.8 \text{ g mol}^{-1}$ was purchased from Biopptide Co. The pure DPPC

multibilayer film and the DPPC multibilayer film inserted with amyloid peptide 1–40 were supported on silicon wafers. The amyloid peptide was dissolved first in HFIP (1,1,1,3,3,3-hexafluoro-2-propanol) and incubated at $T = 298 \text{ K}$. The incubating time was over 12 h to make sure the amyloid peptide disaggregated completely. HFIP was then removed by lyophilization for 12 h. Subsequently, the DPPC and amyloid peptide were dissolved in methanol at 10 to 1 weight ratio. The mixtures were cast on to silicon wafers by dripping, then the methanol was removed by evaporation. Finally, these samples were put in a chamber with saturated water vapor at $T = 328 \text{ K}$ for 8 h and cooled down to $T = 298 \text{ K}$ slowly. All the GISAXS data were collected on BL17B3 (Lai *et al.*, 2006) at the National Synchrotron Radiation Research Center, Hsinchu, Taiwan. The GISAXS data were collected using a two-dimensional detector. The incident angle was fixed at around 0.25° . The energy of the incident X-rays was 10 keV and the sample-to-detector distance was 2.8 m.

3. Results and discussion

Fig. 1 shows the two-dimensional GISAXS intensity distributions from the pure DPPC multibilayer film cast on a silicon wafer at about 306 K at different relative humidities (RH): (A) RH = 36%, (B) RH = 81.38%, (C) RH = 85.58%, (D) RH = 88.2%, (E) RH = 90.2% and (F) RH = 93.88%. These samples were kept in a temperature- and humidity-controlled chamber. When the humidity-controlled sample chamber was left open, the humidity was 36%. As shown in Fig. 1(A), the first-order Bragg peak from the multibilayer film at 36% humidity was around $Q_z = 0.109 \text{ \AA}^{-1}$. Q_z is the component of the scattering vector in the vertical direction to the film and is given by $(4\pi/\lambda) \sin(\theta/2)$, where λ is the incident X-ray wavelength and θ is the scattering angle. This means that the DPPC bilayer thickness is about 58 \AA as calculated from $2\pi/Q_z$. After closing the humidity-controlled

sample chamber door, the relative humidity inside the chamber increased rapidly to about 80%, then steadily increased to 94% in about one hour at a constant temperature of 306 K. The GISAXS data were collected at every 30 s to observe the swelling process. As shown in Fig. 1(B) to Fig. 1(F), the ripple phase appeared once the humidity was raised. At the same time, each Bragg peak split into two peaks. Fig. 2(a) shows intensity profiles with three pixels width from the beam center along the vertical direction for the pure DPPC multibilayers. For the case in which the humidity was 81.38%, the higher intensity first-order Bragg peak is located at $Q = 0.102 \text{ \AA}^{-1}$ and the lower intensity first-order Bragg peak is located at around 0.108 \AA^{-1} . Since the Q value of the lower intensity peak is very close to the Q value of the original first-order Bragg peak at 36% humidity, this peak should correspond to the less swollen bilayers at the bottom of the film. The higher intensity peak should correspond to the more swollen bilayers at the top of the film. As the humidity continued to increase and more time elapsed, both the top layers and the bottom layers seemed to swell steadily and their corresponding diffraction

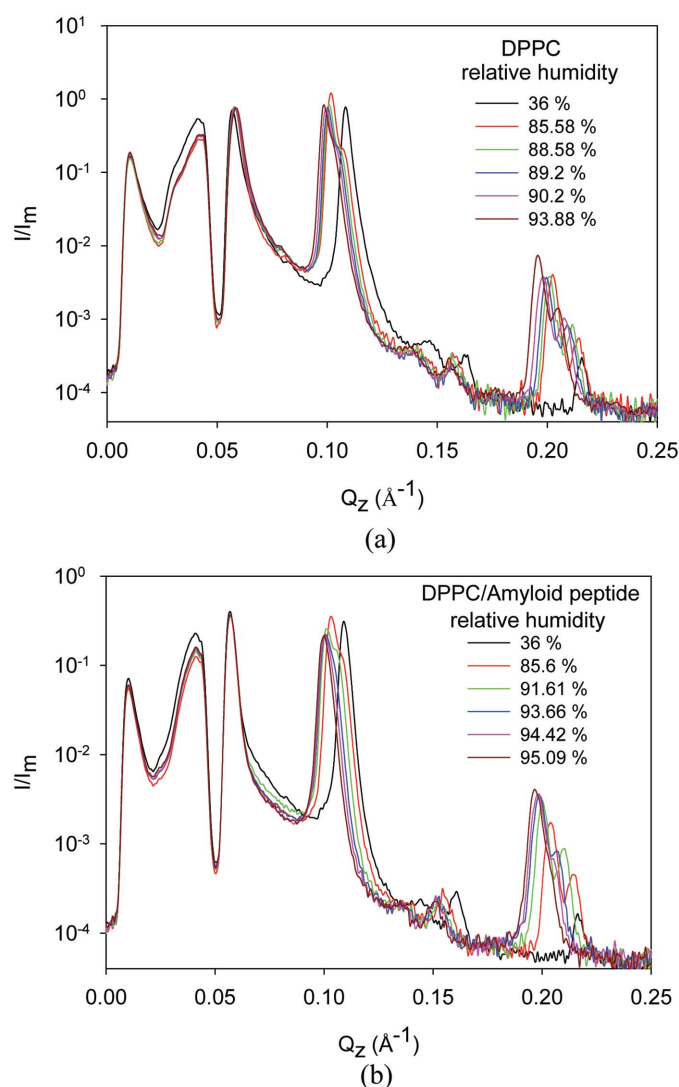


Figure 2
(a) Profiles formed by cuts with three pixels width from the beam center along the vertical direction for the pure DPPC film under different relative humidities at 306 K. The first-order Bragg peaks are around $Q_z = 0.1 \text{ \AA}^{-1}$ and the second-order peak was around $Q_z = 0.2 \text{ \AA}^{-1}$. (b) Profiles formed by cuts with three pixels width from the beam center along the vertical direction for DPPC multibilayers inserted with β -amyloid peptide 1-40 under different relative humidities at 306 K.

peaks all shifted gradually to lower Q values. At 93.88% humidity, the higher and lower intensity peaks have Q values of 0.0985 and about 0.104 \AA^{-1} , respectively. This would correspond to bilayer thicknesses of 64.6 and about 60.4 \AA , respectively, for the higher and lower intensity peaks.

It is estimated that the prepared DPPC multibilayer film has a thickness around 9 \mu m with more than 1500 bilayers (calculated from the amounts of DPPC and the area of the film). The bilayers next to or near to the silicon solid surface could not expand or change their structural arrangements easily compared with the bilayers in the upper part of the film, which might be due to the tight binding to the silicon substrate. Continuous swelling across the film thickness was not seen; instead a bimodal swelling was observed in which one state (the upper layer) had a higher water content and the other state (the lower layer) had a low water content. With sufficient humidity, the ripple phase can be formed, probably by the upper layer which is

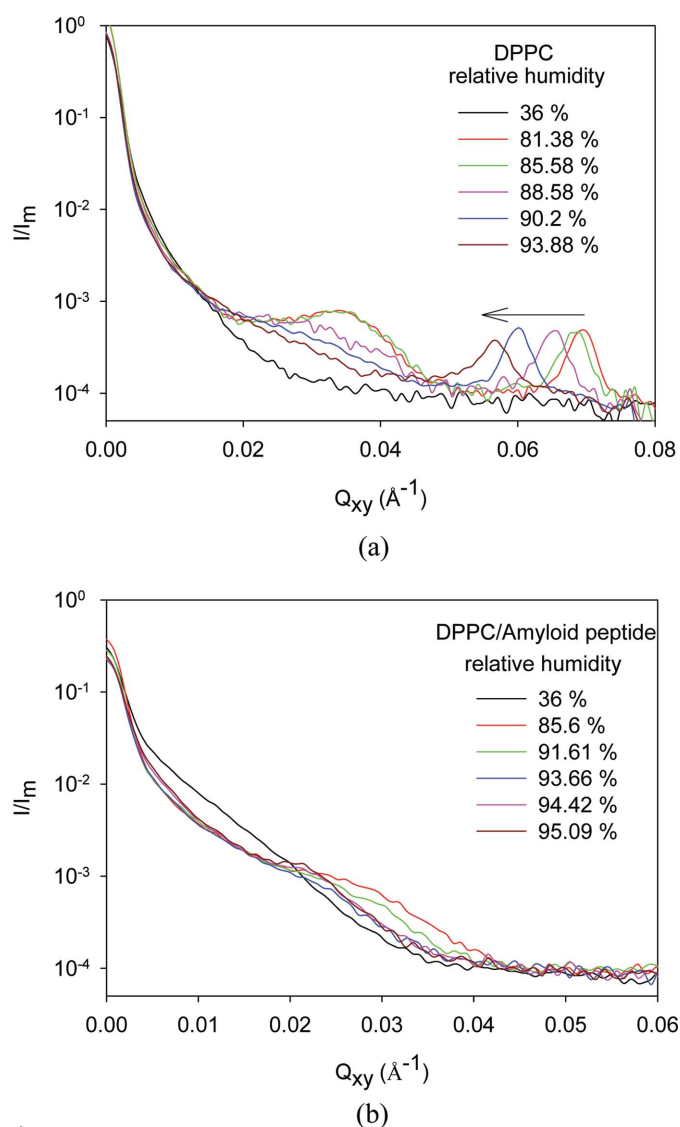


Figure 3
(a) The intensity distribution profiles cut along the lateral direction at the first-order Bragg peak position for a pure DPPC film under different relative humidities at 306 K. The cut lines are shown in Fig. 1. (b) The intensity distribution profiles cut along the lateral direction at the first-order Bragg peak position for DPPC multibilayers inserted with β -amyloid peptide 1-40 under different relative humidities at 306 K. The cut lines are shown in Fig. 4.

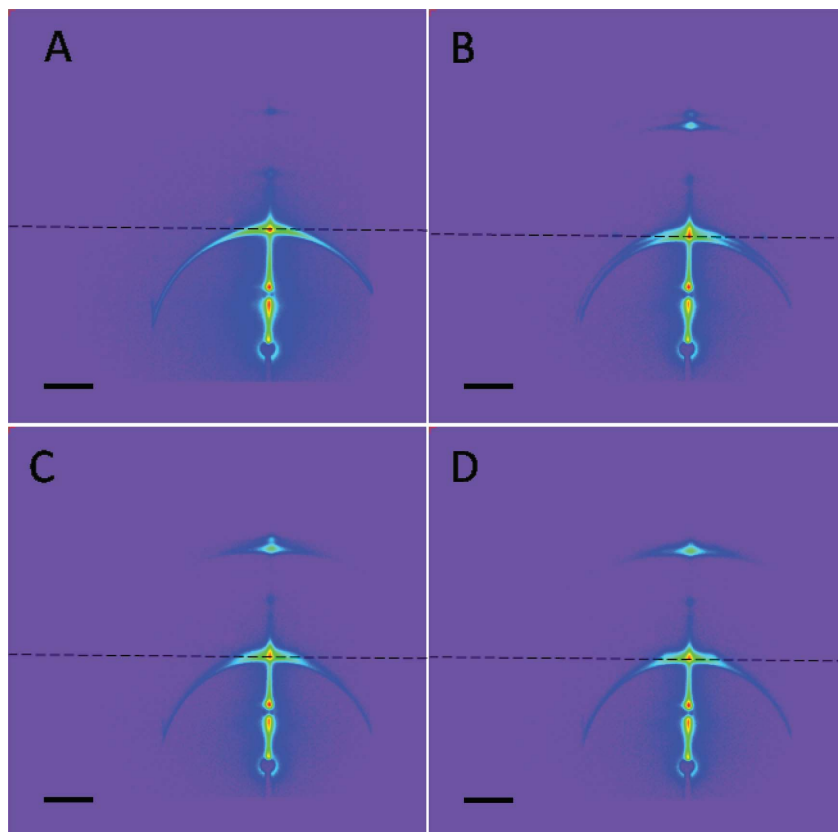


Figure 4
Grazing-incidence X-ray scattering patterns of DPPC multibilayers inserted with β -amyloid peptide 1–40 on a silicon wafer at about 306 K under different relative humidities: (A) RH = 36%, (B) RH = 85.6%, (C) RH = 93.66% and (D) RH = 95.09%. The weight ratio of β -amyloid peptide to DPPC is 10 to 1. The dashed lines are the cuts for the intensity distribution profiles shown in Fig. 3(b). The length of the scale bar is 2.5 cm.

better hydrated. Powder rings can also be observed in the GISAXS two-dimensional patterns, which are due to defects in the bilayers (onion-shaped structures). The small diffraction peaks that appear around $Q = 0.15 \text{ \AA}^{-1}$ in Fig. 2(a) are the first-order Bragg peaks from the specular reflection beam. These peaks are much weaker than the Bragg peaks from the incident beam, which indicates that the reflected beam is much weaker than the incident beam due to the attenuation through the lipid film.

Fig. 3(a) shows the intensity distributions in Q_{xy} along the first ripple phase peak positions. The cutting lines are shown in Fig. 1. During the swelling process, the ripple phase peaks also shifted gradually from $Q_{xy} = 0.07$ to 0.057 \AA^{-1} as the humidity increased from 81.38 to 93.88%. With more hydration, the ripple structure can become more relaxed and the repeat distance of the ripples is increased. The broad peaks occurring at around $Q_{xy} = 0.3$ to 0.4 \AA^{-1} are from the powder ring and they gradually disappeared as the humidity increased.

Similar measurements were carried out for the DPPC multibilayer film inserted with $A\beta$. The measured GISAXS patterns are shown in Fig. 4. The powder rings are more obvious than in the pure DPPC case. This indicates that more onion-like structures are formed in the film due to the insertion of $A\beta$ that might change the spontaneous curvature and flexibility of the DPPC bilayer. The swelling is also a bimodal process as more clearly shown in Fig. 2(b) for the intensity distribution along the vertical line. The first-order Bragg peak moved from $Q = 0.109$ to 0.103 \AA^{-1} (for the higher intensity peak) as the humidity changed from 36 to 85.6%. As the humidity further increased to around ~94–95%, the higher intensity peak moved to $Q =$

0.10 \AA^{-1} . The swollen bilayer thickness for the upper layer seemed to be slightly smaller in the case of the insertion of $A\beta$ at similar humidity conditions. The diffraction peaks from the ripple structure for the DPPC film with $A\beta$ insertion are only barely visible in the two-dimensional pattern of Fig. 4(B) at 85.6% humidity and eventually disappeared at higher humidity. The insertion of $A\beta$ would disturb the bilayer structure and make the bilayer more disordered. There is also a big difference due to the insertion of $A\beta$. Although the swelling process is bimodal for both cases, for the case with $A\beta$ insertion, the smaller first-order Bragg peak originating from the bottom layer of the film gradually disappeared as the humidity increased and time elapsed. This means water vapor can penetrate more easily into the DPPC bilayers inserted with $A\beta$ than into the pure DPPC bilayers.

Fig. 5 compares the scattering profiles at the first-order Bragg peak for the pure DPPC film and the DPPC/amyloid film along the lateral direction at a humidity of 36%. A broad diffuse structure factor in the region of $Q_{xy} = 0.005$ to 0.03 \AA^{-1} for the case with $A\beta$ insertion can be identified by comparing these two scattering profiles. The existence of the diffuse structure factor indicates that the insertion of $A\beta$ induces in-plane structural correlation. The transitions of this in-plane structure factor are shown in Fig. 3(b) as the humidity increased from 36 to 85.6%.

As the humidity increases, this in-plane structure factor shrinks slightly to a smaller Q value, *i.e.* decays faster with increasing Q . This diffuse scattering structure factor could be due to the scattering from the clusters of the inserted amyloid peptides. As found by AFM studies, amyloid peptides could form multimeric channel-like structures in lipid bilayers (Lin *et al.*, 2001). The multimeric channel-like structures can be approximately modeled as a cylinder sitting vertically in the bilayer. We employed the cylinder structural model to fit the diffuse structure profile for the 93.66% relative humidity case. For

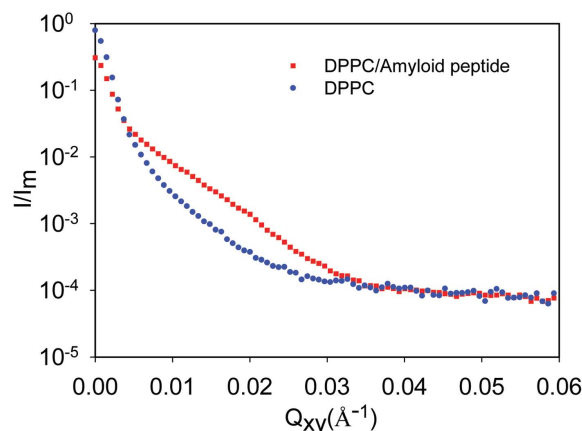


Figure 5
These two profiles were cut from the first-order Bragg peak along the lateral direction at RH = 36%.

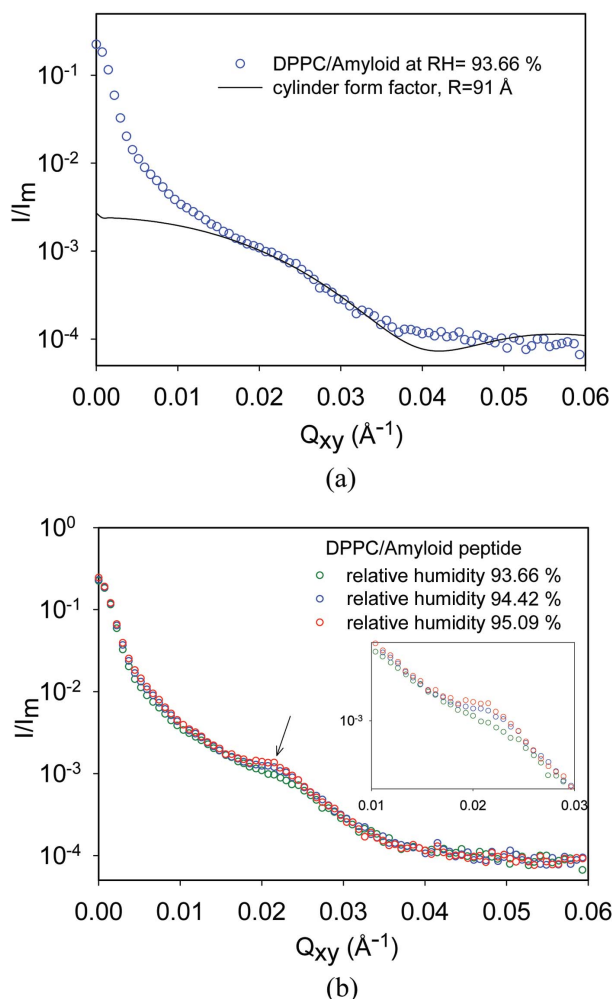


Figure 6
 (a) The intensity distribution profile cut along the lateral direction at the first-order Bragg peak position for DPPC multibilayers inserted with β -amyloid peptide 1–40 at 93.66% relative humidity at 306 K. The solid line is the fitting of the diffuse structure profile according to a form factor corresponding to cylinders sitting vertically in the bilayer. (b) The intensity distribution profiles cut along the lateral direction at the first-order Bragg peak position for DPPC multibilayers inserted with β -amyloid peptide 1–40 under higher relative humidity at 306 K. The inset shows the development of the hump as the relative humidity increases.

vertical cylinders, the scattering intensity profile in the lateral direction is given by (Lin *et al.*, 1987)

$$I(Q) = (\Delta\rho)^2 V^2 \left(\frac{2J_1(QR)}{QR} \right)^2, \quad (1)$$

where $\Delta\rho$ is the X-ray scattering length density difference, V is the volume of the cylinder and R is the radius of the cylinder. As shown in Fig. 6(a), the in-plane structure factor can be fitted with the cylinder form factor of equation (1). The radius of the cylinder is found to be 91 ± 1 Å. The AFM studies of Lin *et al.* (2001) showed that the channel-like structures of oligomeric $A\beta$ 1–42 have an outer diameter of 8–12 nm. The diameter of the cylindrical $A\beta$ 1–40 cluster obtained in this study is about 18 nm, which is slightly larger than the amyloid cluster size observed by AFM for the $A\beta$ 1–42 cluster. The difference in size could be due to different types of amyloid peptides, concentration effects or swelling effects. As shown in Fig. 6(b), when the relative humidity exceeds about 94%, a small hump around $Q = 0.021$ Å⁻¹ is also observed. The appearance of the hump might

indicate the in-plane ordering of $A\beta$ clusters at sufficient hydration of the bilayers. The spacing d between the $A\beta$ clusters would be around 300 Å (estimated from $2\pi/Q$). On average, the number of DPPC molecules per $A\beta$ cluster will be about 700. The interfacial area A per DPPC lipid ranges from 56 to 72 Å². (Tristram-Nagle *et al.*, 1993; Nagle, 1993) and a mean value of 64 Å² is used in estimating the DPPC-to- $A\beta$ cluster ratio by $[(\pi d^2/4) - \pi R^2]/A \simeq 700$. The weight ratio of lipid to peptide that we employed in this study was 10 to 1, so the molar ratio of lipid to peptide was about 60 to 1. This means the number of $A\beta$ molecules in one cluster would be about $700/60 \simeq 12$. On average, each $A\beta$ cluster would occupy an interface area of about 22 nm². This value is very close to that observed by AFM studies (Lin *et al.*, 2001).

4. Conclusions

In this study of the swelling of the pure DPPC multibilayer film and the DPPC multibilayer film inserted with $A\beta$, it was found that the hydration process was bimodal with a better-hydrated top layer and a less-hydrated bottom layer. The gel-to-ripple phase transition suffers a strong confinement effect due to the presence of the solid substrate. With the insertion of $A\beta$, the ripple phase of the membrane bilayers was suppressed at high humidity and the whole film can be swollen more uniformly at lower incubation time than the pure DPPC film supported on a silicon wafer. This means water vapor can penetrate more easily into the DPPC bilayers inserted with $A\beta$ than into the pure DPPC bilayers. From analyzing the diffuse scattering around the Bragg peak in the lateral direction, the amyloid peptide molecules are found to form clusters in the bilayer with a radius of about 9 nm. It is also estimated that the number of $A\beta$ molecules in one cluster is about 12 and on average each $A\beta$ cluster occupies an interface area of about 4.6 nm square. As the relative humidity exceeds about 94%, the $A\beta$ clusters seem to develop an ordered structure with a spacing of about 300 Å.

We would like to thank the NSRRC for the beam time and support during the measurements. This research is supported by the National Science Council, ROC, grant Nos. NSC94-2113-M-007-003 and NSC95-2623-7-007-012-NU.

References

- Ege, C. & Lee, K. Y. C. (2004). *Biophys. J.* **87**, 1732–1740.
 Huang, T. H. J., Yang, D.-S., Plaskos, N. P., Go, S., Yip, C. M., Fraser, P. E. & Chakrabarty, A. (2000). *J. Mol. Biol.* **297**, 73–87.
 Jeng, U. S., Hsu, C.-H., Lin, T.-L., Wu, C. M., Chen, H.-L., Tai, L. A. & Hwang, K. C. (2005). *Physica B*, **357**, 193–198.
 Jeng, U. S., Hsu, C. H., Sun, Y. S., Lai, Y. H., Chung, W. T., Sheu, H. S., Lee, H. Y., Song, Y. F., Liang, K. S. & Lin, T. L. (2005). *Macromol. Res.* **13**, 506–513.
 Ji, S. R., Wu, Y. & Sui, S. F. (2002). *Biochemistry (Moscow)*, **67**, 1283–1288.
 Koltover, I., Salditt, T., Rigaud, J.-L. & Safinya, C. R. (1998). *Phys. Rev. Lett.* **81**, 2494–2497.
 Lai, Y. H., Sun, Y. S., Jeng, U., Lin, J. M., Lin, T.-L., Shen, H.-S., Chuang, W.-T., Huang, Y.-S., Hsu, C.-H., Lee, M.-T., Lee, H.-Y., Liang, K.-S., Gabriel, A. & Koch, M. H. J. (2006). *J. Appl. Cryst.* **39**, 871–877.
 Lee, B., Park, I., Yoon, J., Park, S., Kim, J., Kim, K.-W., Chang, T. & Ree, M. (2005). *Macromolecules*, **38**, 4311–4323.
 Li, L., Darden, T. A., Bartolotti, L., Kominos, D. & Pedersen, L. G. (1999). *Biophys. J.* **76**, 2871–2878.
 Lin, H., Bhatia, R. & Lal, R. (2001). *FASEB J.* **15**, 2433–2444.
 Lin, T.-L., Chen, S.-H., Gabriel, N. E. & Roberts, M. F. (1987). *J. Phys. Chem.* **91**, 406–413.

conference papers

- Lomakin, A., Chung, D. S., Benedek, G. B., Kirschner, D. A. & Teplow, D. B. (1996). *Proc. Natl Acad. Sci. USA*, **93**, 1125–1129.
- Nagle, J. F. (1993). *Biophys. J.* **64**, 1476–1481.
- Salditt, T., Metzger, T. H. & Peisl, J. (1994). *Phys. Rev. Lett.* **73**, 2228–2231.
- Salditt, T., Vogel, M. & Fenzl, W. (2003). *Langmuir*, **19**, 7703–7711.
- Spaar, A., Munster, C. & Salditt, T. (2004). *Biophys. J.* **87**, 396–407.
- Trisram-Nagle, S., Zhang, R., Suter, R. M., Worthington, C. R., Sun, W.-J. & Nagle, J. F. (1993). *Biophys. J.* **64**, 1097–1109.
- Vogel, M., Münster, C., Fenzl, W., Thiaudère, D. & Salditt, T. (2000). *Physica B*, **283**, 32–36.
- Wood, S. J., Maleeff, B., Hart, T. & Wetzel, R. (1996). *J. Mol. Biol.* **256**, 870–877.